Available online at www.sciencedirect.com
SCIENCE DIRECT®
Journal of Sound and Vibration 271 (2004) 685–703
JOURNAL OF SOUND AND VIBRATION
www.elsevier.com/locate/jsvi

Spectral analysis for the transverse vibration of an axially moving Timoshenko beam

Usik Lee*, Joohong Kim, Hyungmi Oh

Department of Mechanical Engineering, Inha University, 253 Yonghyun-Dong, Nam-Ku, Incheon 402-751, South Korea

Received 18 June 2002; accepted 13 March 2003

Abstract

The use of frequency-dependent spectral element matrix (or exact dynamic stiffness matrix) in structural dynamics is known to provide very accurate solutions, while reducing the number of degrees of freedom to resolve the computational and cost problems. Thus, in the present paper, the spectral element model is formulated for the axially moving Timoshenko beam under a uniform axial tension. The high accuracy of the present spectral element is then verified by comparing its solutions with the conventional finite element solutions and exact analytical solutions. The effects of the axial velocity and axial tension on the vibration characteristics, the dispersion relation, and the stability of a moving Timoshenko beam are analytically and numerically investigated.

1. Introduction

Axially moving structures are of technological importance and present in a wide class of engineering problems which arise in industrial, mechanical, civil, aerospatial, automotive and electronic applications in the form of threadlines in the textile industry, chain and belt drives, high-speed paper and magnetic tapes, band saw blades, fiber winding, filaments, aerial cable tramways, cooling tower strips and the like. Recent developments in research on axially moving structures have been reviewed by Wickert and Mote [1] and Pellicano and Vestrani [2].

The axial velocity of a structure may significantly affects the dynamic characteristics of the structure even at low velocity, giving rise to variations of natural frequencies and complex modes. Above a certain critical axial velocity, the axially moving structures may experience severe vibrations and structural instability to result in structural failures. Thus, it is very important to

*Corresponding author. Tel.: +82-32-860-7318.
E-mail address: ulee@inha.ac.kr (U. Lee).

0022-460X/03/$ - see front matter © 2003 Elsevier Ltd. All rights reserved.
doi:10.1016/S0022-460X(03)00300-6

accurately predict the dynamic characteristics and instability of such structures in advance for the successful analysis and optimal design of a broad class of technological devices.

The axially moving beam-like one-dimensional structure with flexural rigidity has been traditionally represented by the linear or non-linear Euler–Bernoulli beam theory [2–26] by assuming that the beam is relatively thin as compared with its length. It appears that, to the authors' knowledge, there have been very few studies on the axially moving beam-like one-dimensional structures in which Timoshenko beam theory was used. It is in this context that the structure theory considered in this paper is the Timoshenko beam theory. Simpson [27] was probably the first to derive the equations of motion for the moving thick beam on the basis of the Timoshenko beam theory, but no numerical results were given. Later, Chonan [28] studied the steady state response of a moving Timoshenko beam by applying Laplace transform method. Simpson [27] did not consider the axial tension in their equations.

The solutions of the equations of motion for moving beams have been obtained by various solution techniques including the Galerkin's method [2–9], assumed mode method [10], finite element method (FEM) [11,12], Green's function method [13], transfer function method [14], perturbation method [15–17], asymptotic method [18,19], and the Laplace transform method [28]. In the literature [29,30], it has been well recognized that the spectral element method (SEM) is one of very accurate solution methods for the dynamic analysis of structures. In SEM, the spectral element matrix (or exact dynamic stiffness matrix) is formulated in frequency-domain by using exact dynamic shape functions. Therefore, it does not require any structural discretization to improve the solution accuracy for a uniform beam, regardless of its length. As it is one of element methods, the conventional finite element assembly procedure can be equally applied to formulate the global system dynamic equation of a structure. In SEM, the dynamic responses in frequency- and time-domains are computed very efficiently by using the forward-FFT (simply, FFT) and inverse-FFT (simply, IFFT) algorithms. Recently, Le-Ngoc and McCallion [31] derived the dynamic stiffness matrix for the axially moving string to obtain exact eigenvalues.

The purposes of the present paper are first to formulate the spectral element model for the transverse vibration of an axially moving Timoshenko beam subjected to a constant axial tension, and then to verify its high accuracy by comparing with the solutions by the other solutions methods, and finally to investigate the effects of the axial velocity and the axial tension on the vibration and stability of a moving beam.

2. Equations of motion

Consider a beam of flexural rigidity EI and shear rigidity κGA, which travels under an applied axial tension P with constant axial velocity c. Based on the Timoshenko beam theory [32], the total transverse deflection and the angle of rotation due to bending are denoted by $w(x,t)$ and $\psi(x,t)$, respectively. The total kinetic and potential energies are given by

$$T = \frac{1}{2}\int_0^L \{\rho A[c^2 + (\dot{w} + cw')^2] + \rho I(\dot{\psi} + c\psi')^2\}\,\mathrm{d}x,$$

$$V = \frac{1}{2}\int_0^L \{EI\,\psi'^2 + \kappa GA(w' - \psi)^2 + Pw'^2\}\,\mathrm{d}x, \tag{1}$$

where L is the length of beam, ρA is the mass per length, ρI is the mass moment of inertia per length, and κ is the numerical factor depending of the shape of the cross-section. In Eq. (1), the dot $(\cdot)$ denotes the derivative with respective to time and the prime $(')$ denotes the derivative with respective to spatial co-ordinate x. Define the shear force $Q(x)$ and the bending moment $M(x)$ as

$$\begin{aligned} Q(x) &= \kappa GA(w' - \psi) - \rho Ac(\dot{w} + cw') + Pw', \\ M(x) &= -EI\,\psi' + \rho Ic(\dot{\psi} + c\psi'). \end{aligned} \tag{2}$$

The virtual work due to the external force $p(x, t)$ and boundary shear forces and bending moments are given by

$$\delta W = \int_0^L p(x,t)\delta w\,\mathrm{d}x + M_1\delta\psi_1 + M_2\delta\psi_2 + Q_1\delta w_1 + Q_2\delta w_2. \tag{3}$$

Introducing Eqs. (1) and (3) into the extended Hamilton's principle

$$\int_{t_1}^{t_2} (\delta T - \delta V + \delta W)\,\mathrm{d}t = 0 \tag{4}$$

gives

$$\begin{aligned} &\int_{t_1}^{t_2}\int_0^L \left\{\frac{\partial}{\partial x}[\kappa GA(w' - \psi)] - \rho A(c^2 w'' + 2c\dot{w}' + \ddot{w}) + Pw'' + p(x,t)\right\}\delta w\,\mathrm{d}x\,\mathrm{d}t \\ &\quad + \int_{t_1}^{t_2}\int_0^L \left\{\frac{\partial}{\partial x}(EI\psi') - \rho I(c^2\psi'' + 2c\dot{\psi}' + \ddot{\psi}) + \kappa GA(w' - \psi)\right\}\delta\psi\,\mathrm{d}x\,\mathrm{d}t \\ &\quad + \int_{t_1}^{t_2} [-Q(x)\delta w|_0^L + Q_1\delta w_1 + Q_2\delta w_2]\,\mathrm{d}t \\ &\quad + \int_{t_1}^{t_2} [M(x)\delta\psi|_0^L + M_1\delta\psi_1 + M_2\delta\psi_2]\,\mathrm{d}t = 0. \end{aligned} \tag{5}$$

From Eq. (5), the equations of motion for the uniform Timoshenko beam can be derived as

$$\begin{aligned} &\kappa GA(w'' - \psi') - \rho A(c^2 w'' + 2c\dot{w}' + \ddot{w}) + Pw'' + p(x,t) = 0, \\ &EI\,\psi'' - \rho I(c^2\psi'' + 2c\dot{\psi}' + \ddot{\psi}) + \kappa GA(w' - \psi) = 0. \end{aligned} \tag{6}$$

The relevant boundary conditions are specified in terms of any pair of conditions selected from the following groups:

$$\begin{aligned} &\{w(0) = w_1 \quad \text{or} \quad Q(0) = -Q_1\}, \quad \{\psi(0) = \psi_1 \quad \text{or} \quad M(0) = M_1\} \quad \text{at } x = 0, \\ &\{w(L) = w_2 \quad \text{or} \quad Q(L) = Q_2\}, \quad \{\psi(L) = \psi_2 \quad \text{or} \quad M(L) = -M_2\} \quad \text{at } x = L. \end{aligned} \tag{7}$$

3. Spectral element formulation

The spectral element formulation begins with the governing equations of motion without external forces [29]. The free vibration response of the moving Timoshenko beam are then

represented in the spectral forms as

$$w(x,t)=\sum_{n=1}^{N} W_n(x)\mathrm{e}^{\mathrm{i}\omega_n t},\quad \psi(x,t)=\sum_{n=1}^{N}\Psi_n(x)\mathrm{e}^{\mathrm{i}\omega_n t}, \tag{8}$$

where $W_n(x)$ and $\Psi_n(x)$ are the spectral components (or Fourier coefficients) corresponding to the discrete frequencies $\omega_n=2\pi n/T$ $(n=1,2,\ldots,N)$. N denotes the number of spectral components to be taken into account in the analysis, and T is the time window related to N as

$$N=2f_{NYQ}T \tag{9}$$

where f_{NYQ} is the Nyquist frequency in Hz. The accuracy of time responses may depend on how many spectral components are taken into account in the analysis. The summation and subscripts used in Eq. (8) are so obvious that they will be omitted in the following equations for brevity.

By substituting Eq. (8) into Eq. (6), with $p(x,t)=0$, and by following the spectral analysis procedure by Doyle [29], one may obtain

$$\begin{aligned}&(1+a_4-a_1c^2)W''-a_1 2\mathrm{i}c\omega W'+a_1\omega^2 W-\Psi'=0,\\&(1-a_2c^2)\Psi''-a_2 2\mathrm{i}c\omega\Psi'+(a_2\omega^2-a_3)\Psi+a_3W'=0,\end{aligned} \tag{10}$$

where $\mathrm{i}=\sqrt{-1}$ and a_m $(m=1,2,3,4)$ are defined as

$$a_1=\frac{\rho A}{\kappa GA},\quad a_2=\frac{\rho I}{EI},\quad a_3=\frac{\kappa GA}{EI},\quad a_4=\frac{P}{\kappa GA}. \tag{11}$$

The general solutions of Eq. (10) (i.e., spectral components) are assumed in the forms

$$W(x)=\bar{W}\mathrm{e}^{\mathrm{i}kx},\quad \Psi(x)=\bar{\Psi}\mathrm{e}^{\mathrm{i}kx}, \tag{12}$$

where k is the wavenumber. Substituting Eq. (12) into Eq. (10) yields an eigenvalue problem as

$$\begin{bmatrix}(1+a_4-a_1c^2)k^2-2a_1c\omega k-a_1\omega^2 & \mathrm{i}k\\ -\mathrm{i}a_3k & (1-a_2c^2)k^2-2a_2c\omega k-(a_2\omega^2-a_3)\end{bmatrix}\begin{Bmatrix}\bar{W}\\ \bar{\Psi}\end{Bmatrix}=\begin{Bmatrix}0\\0\end{Bmatrix}. \tag{13}$$

From the condition for the existence of non-trivial solutions of Eq. (13), the dispersion relation can be derived as follows:

$$k^4+\alpha k^3+\beta k^2+\gamma k+\eta=0, \tag{14}$$

where

$$\begin{aligned}\alpha&=-2c\omega(a_1+a_2+a_2a_4-2a_1a_2c^2)/\Delta,\\ \beta&=[a_3(a_4-a_1c^2)-(a_1+a_2+a_2a_4-6a_1a_2c^2)\omega^2]/\Delta,\\ \gamma&=2c\omega a_1(2a_2\omega^2-a_3)/\Delta,\\ \eta&=\omega^2a_1(a_2\omega^2-a_3)/\Delta,\\ \Delta&=(1-a_2c^2)(1+a_4-a_1c^2).\end{aligned} \tag{15}$$

By using the four roots of Eq. (14), the general solutions of Eq. (10) can be expressed as

$$W(x) = \sum_{r=1}^{4} A_r e^{ik_r x}, \quad \Psi(x) = \sum_{r=1}^{4} \varepsilon_r A_r e^{ik_r x}, \tag{16}$$

where

$$\varepsilon_r = \frac{a_3 i k_r}{(1 - a_2 c^2)k_r^2 - 2a_2 c\omega k_r - (a_2\omega^2 - a_3)} \quad (r = 1, 2, 3, 4). \tag{17}$$

Now, consider a finite beam element of length l as shown in Fig. 1. The spectral nodal displacement degrees of freedom (simply, spectral nodal d.o.f.s) in Fig. 1 are defined by

$$W_1 = W(0), \quad \Psi_1 = \Psi(0), \quad W_2 = W(l), \quad \Psi_2 = \Psi(l). \tag{18}$$

Substituting Eq. (16) into Eq. (18) gives a relation between the spectral nodal d.o.f.s vector $\{\mathbf{y}\}$ and the constants vector $\{\mathbf{A}\}$ as

$$\{\mathbf{d}\} = [\mathbf{X}(\omega)]\{\mathbf{A}\}, \tag{19}$$

where

$$\{\mathbf{d}\} = \begin{Bmatrix} W_1 & \Psi_1 & W_2 & \Psi_2 \end{Bmatrix}^{\mathrm{T}},$$
$$\{\mathbf{A}\} = \begin{Bmatrix} A_1 & A_2 & A_3 & A_4 \end{Bmatrix}^{\mathrm{T}},$$
$$[\mathbf{X}(\omega)] = \begin{bmatrix} 1 & 1 & 1 & 1 \\ \varepsilon_1 & \varepsilon_2 & \varepsilon_3 & \varepsilon_4 \\ e_1 & e_2 & e_3 & e_4 \\ e_1\varepsilon_1 & e_2\varepsilon_2 & e_3\varepsilon_3 & e_4\varepsilon_4 \end{bmatrix} \tag{20}$$

with

$$e_r = e^{ik_r l} \quad (r = 1, 2, 3, 4). \tag{21}$$

By substituting Eq. (8) into Eq. (5), the spectral force–displacement relations can be obtained as

$$Q = \kappa GA[(1 + a_4 - a_1 c^2)W' - a_1 ic\omega W - \Psi],$$
$$M = -EI[(1 - a_2 c^2)\Psi' - a_2 ic\omega\Psi]. \tag{22}$$

In Eq. (22), the subscripts n used for Q and M, which represent the nth spectral components, are omitted for brevity. The spectral nodal shear forces and bending moments specified on the two ends of beam element, as shown in Fig. 1, are defined by

$$Q_1 = -Q(0), \quad M_1 = M(0), \quad Q_2 = Q(l), \quad M_2 = -M(l). \tag{23}$$

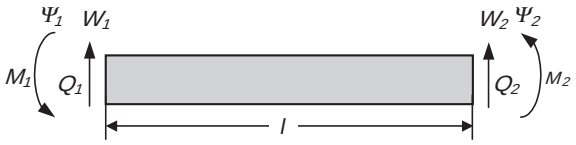

Fig. 1. Sign convention for the finite Timoshenko-beam element.

Substituting Eq. (16) into Eq. (23) gives a relation between the spectral nodal forces vector $\{\mathbf{f}\}$ and the constants vector $\{\mathbf{A}\}$ as

$$\{\mathbf{f}\} = [\mathbf{Y}(\omega)]\{\mathbf{A}\}, \tag{24}$$

where

$$\{\mathbf{f}\} = \{\, Q_1 \quad M_1 \quad Q_2 \quad M_2 \,\}^{\mathrm{T}},$$
$$[\mathbf{Y}(\omega)] = EI \begin{bmatrix} -g_1 & -g_2 & -g_3 & -g_4 \\ -h_1 & -h_2 & -h_3 & -h_4 \\ e_1 g_1 & e_2 g_2 & e_3 g_3 & e_4 g_4 \\ e_1 h_1 & e_2 h_2 & e_3 h_3 & e_4 h_4 \end{bmatrix} \tag{25}$$

with

$$g_r = \mathrm{i}a_3[(1 + a_4 - a_1 c^2)k_r - a_1 c\omega + \mathrm{i}\varepsilon_r],$$
$$h_r = \mathrm{i}[(1 - a_2 c^2)k_r - a_2 c\omega]\varepsilon_r \quad (r = 1, 2, 3, 4). \tag{26}$$

Eliminating the constants vector $\{\mathbf{A}\}$ from Eqs. (19) and (24) gives the nodal forces-nodal displacements relation as

$$\{\mathbf{f}\} = [\mathbf{s}(\omega)]\{\mathbf{d}\}, \tag{27}$$

where $[\mathbf{s}(\omega)]$ is the spectral element matrix, which is the frequency-dependent symmetric matrix defined by

$$[\mathbf{s}(\omega)] = [\mathbf{Y}(\omega)][\mathbf{X}(\omega)]^{-1}. \tag{28}$$

The spectral element matrices can be assembled in a completely analogous way to that used in FEM. Applying the boundary conditions after the assembly may provide a global system equation in the form as

$$[\mathbf{S}(\omega)]\{\mathbf{d}_g\} = \{\mathbf{f}_g\}, \tag{29}$$

where $[\mathbf{S}(\omega)]$ is the global spectral matrix (i.e., global dynamic stiffness matrix), $\{\mathbf{d}_g\}$ is the global spectral nodal d.o.f.s vector, and $\{\mathbf{f}_g\}$ is the global spectral nodal forces vector.

To obtain the dynamic responses in time-domain, first compute $\{\mathbf{f}_g\}$ from the external forces transformed into the frequency-domain by using the forward FFT algorithm. Next solve Eq. (29) for $\{\mathbf{d}_g\}$ and apply the results into Eq. (19) to compute the spectral displacement components from Eq. (16). Finally, based on Eq. (8), the inverse FFT algorithm is used to obtain the dynamic responses in the time-domain. The natural frequencies ω_{NAT} are computed from the condition that the determinant of global spectral matrix $[\mathbf{S}(\omega)]$ becomes zero as follows:

$$\det[\mathbf{S}(\omega)] = 0. \tag{30}$$

4. Stability of moving beam

An axially moving beam may become unstable if its axial velocity is over a certain critical value. To investigate the stability of the moving beam one usually assume the free vibration responses of

the form [34]

$$w(x,t) = \bar{w}e^{\lambda t}, \quad \psi(x,t) = \bar{\psi}e^{\lambda t}. \tag{31}$$

Applying Eq. (31) into the free vibration equations, Eq. (8) with $p(x,t) = 0$, yields an eigenvalue problem from which the eigenvalues λ can be computed in the form of complex number

$$\lambda \equiv \mathrm{Re}(\lambda) + \mathrm{i}\,\mathrm{Im}(\lambda). \tag{32}$$

The type of instability can be determined from the signs of the real (Re) and imaginary (Im) parts of all eigenvalues λ as follows:

$$\begin{aligned}
&\text{Stable if } \mathrm{Re}(\lambda) \leqslant 0,\\
&\text{Dynamic instability(flutter) if } \mathrm{Re}(\lambda) > 0 \quad \text{and} \quad \mathrm{Im}(\lambda) \neq 0,\\
&\text{Static instability(divergence) if } \mathrm{Re}(\lambda) > 0 \quad \text{and} \quad \mathrm{Im}(\lambda) = 0.
\end{aligned} \tag{33}$$

The eigenvalue problem to investigate the stability of the present moving beam problem can be readily reduced from Eq. (29) by simply replacing $\mathrm{i}\omega$ with λ, which can be hinted from Eqs. (8) and (31), as

$$[\mathbf{S}(\lambda)]\{\mathbf{d}_g\} = \{\mathbf{0}\}. \tag{34}$$

The type of instability, for specific values of axial velocity c and axial tension P, is then determined by investigating the eigenvalues λ numerically solved from the characteristic equation

$$\det[\mathbf{S}(\lambda)] = 0. \tag{35}$$

The wavenumbers k_r $(r = 1, 2, 3, 4)$ required to compute $[\mathbf{S}(\lambda)]$ in Eq. (35) are obtained from Eq. (14), with replacing $\mathrm{i}\omega$ with λ.

The critical axial velocity at which the static instability (i.e., divergence speed c_D) occurs can be analytically derived in a closed form from either the existence of non-trivial equilibrium position (static eigenvalue problem) [13,35] or the observation that the static instability occurs when the axial velocity of a beam equals the propagating wave speed in the beam [35]. In the following, the aforementioned two approaches will be used to determine the divergence speeds for a Timoshenko beam simply supported at both ends.

For the first approach, the static eigenvalue problem can be readily reduced from Eq. (13) by putting $\omega = 0$ as

$$\begin{bmatrix} (1 + a_4 - a_1c^2)k^2 & \mathrm{i}k \\ -\mathrm{i}a_3k & (1 - a_2c^2)k^2 + a_3 \end{bmatrix} \begin{Bmatrix} \bar{W} \\ \bar{\Psi} \end{Bmatrix} = \begin{Bmatrix} 0 \\ 0 \end{Bmatrix}. \tag{36}$$

For the existence of non-trivial solutions of Eq. (36), the following characteristic equation should be satisfied:

$$k^2[(1 + a_4 - a_1c^2)(1 - a_2c^2)k^2 - a_3(a_1c^2 - a_4)] = 0. \tag{37}$$

Eq. (37) gives four characteristic values as

$$k_1 = k_2 = 0, \quad k_3 = -k_4 = \bar{k} = \sqrt{\frac{a_3(a_1c^2 - a_4)}{(1 - a_2c^2)(1 + a_4 - a_1c^2)}}. \tag{38}$$

Thus, the non-trivial equilibrium displacements of the moving beam can be expressed in the form

$$w(x) = A_1 + A_2 x + A_3 e^{i\bar{k}x} + A_3 e^{-i\bar{k}x},$$
$$\psi(x) = B_1 + B_2 x + B_3 e^{i\bar{k}x} + B_3 e^{-i\bar{k}x}, \tag{39}$$

where

$$B_1 = A_2, \quad B_2 = 0, \quad B_3 = \frac{ia_3\bar{k}}{(1 - a_2c^2)\bar{k}^2 + a_3} A_3, \quad B_4 = -\frac{ia_3\bar{k}}{(1 - a_2c^2)\bar{k}^2 + a_3} A_4. \tag{40}$$

The coefficients A_i $(i = 1, 2, 3, 4)$ are determined by the boundary conditions. Applying simply supported at both ends to Eq. (39) gives

$$\bar{k}_n = \frac{n\pi}{L} \quad (n = 1, 2, 3, \ldots), \tag{41}$$

where n denotes the vibration mode number. Equating Eq. (38) with Eq. (41) gives the divergence speed c_{Dn}, at which the divergence instability of the nth vibration mode occurs, as follows:

$$c_{Dn} = \begin{cases} \dfrac{1}{n\pi}\sqrt{\dfrac{q_1 - \sqrt{q_1^2 + q_2}}{2a_1a_2}} & \text{(for bending wave mode)}, \\ \dfrac{1}{n\pi}\sqrt{\dfrac{q_1 + \sqrt{q_1^2 + q_2}}{2a_1a_2}} & \text{(for shear wave mode)}, \end{cases} \tag{42}$$

where

$$q_1 = a_1a_3L^2 + \pi^2n^2(a_1 + a_2 + a_2a_4),$$
$$q_2 = -4\pi^2n^2a_1a_2[a_3a_4L^2 + \pi^2n^2(1 + a_4)]. \tag{43}$$

Now, as the second approach, the divergence speed c_D will be obtained from the observation that the static instability occurs when the axial velocity becomes equal to the phase speed of the bending wave of a stationary beam, i.e., $c_D = c_p$ [35]. The phase speed can be obtained from [29]

$$c_p = \frac{\omega}{k}. \tag{44}$$

The dispersion relation for the stationary beam with zero axial velocity can be reduced from Eq. (14) as

$$k^4 + \bar{\beta}k^2 + \bar{\eta} = 0, \tag{45}$$

where

$$\bar{\beta} = a_3a_4 - \omega^2(a_1 + a_2 + a_2a_4)/\bar{\Delta},$$
$$\bar{\eta} = a_1\omega^2(a_2\omega^2 - a_3)/\bar{\Delta},$$
$$\bar{\Delta} = 1 + a_4. \tag{46}$$

Eq. (45) gives four characteristic values as

$$k_1 = -k_2 = \bar{k}_1 = \sqrt{\frac{-\bar{\beta} + \sqrt{\bar{\beta}^2 - 4\bar{\eta}}}{2}},$$
$$k_3 = -k_4 = \bar{k}_2 = \sqrt{\frac{-\bar{\beta} - \sqrt{\bar{\beta}^2 - 4\bar{\eta}}}{2}}. \tag{47}$$

On the basis of the characteristic values given in Eq. (47), the general solutions of the stationary beam can be obtained as

(a) When $\omega < \omega_c$:

$$W(x) = A_1 \sin(\bar{k}_1 x) + A_2 \cos(\bar{k}_1 x) + A_3 \sinh(\bar{k}_2 x) + A_4 \cosh(\bar{k}_2 x),$$
$$\Psi(x) = b_1 A_2 \sin(\bar{k}_1 x) - b_1 A_1 \cos(\bar{k}_1 x) + b_2 A_3 \sinh(\bar{k}_2 x) + b_2 A_4 \cosh(\bar{k}_2 x). \tag{48}$$

(b) When $\omega = \omega_c$:

$$W(x) = A_1 \sin(\bar{k}_1 x) + A_2 \cos(\bar{k}_1 x) + A_3 + A_4 x,$$
$$\Psi(x) = b_1 A_2 \sin(\bar{k}_1 x) - b_1 A_1 \cos(\bar{k}_1 x) - b_3 A_4. \tag{49}$$

(c) When $\omega > \omega_c$:

$$W(x) = A_1 \sin(\bar{k}_1 x) + A_2 \cos(\bar{k}_1 x) + A_3 \sin(\bar{k}_2 x) + A_4 \cos(\bar{k}_2 x),$$
$$\Psi(x) = b_1 A_2 \sin(\bar{k}_1 x) - b_1 A_1 \cos(\bar{k}_1 x) + b_2 A_4 \sin(\bar{k}_2 x) - b_2 A_3 \cos(\bar{k}_2 x), \tag{50}$$

where

$$b_1 = \frac{a_3 \bar{k}_1}{(a_2\omega^2 - a_3) - \bar{k}_1^2}, \quad b_2 = \frac{a_3 \bar{k}_2}{(a_2\omega^2 - a_3) - \bar{k}_2^2}, \quad b_3 = \frac{a_3}{a_2\omega^2 - a_3} \tag{51}$$

and $\omega_c = \sqrt{a_3/a_2}$ denotes the cut-off frequency below that the second mode (i.e., shear mode) attenuates. Applying simply supported at both ends to Eqs. (48)–(50) gives

(a) When $\omega \leqslant \omega_c$:

$$\bar{k}_{1n} = \frac{n\pi}{L} \quad (n = 1, 2, 3, \ldots). \tag{52}$$

(b) When $\omega > \omega_c$:

$$\bar{k}_{1n} = \frac{n\pi}{L} \quad \text{or} \quad \bar{k}_{2n} = \frac{n\pi}{L} \quad (n = 1, 2, 3, \ldots). \tag{53}$$

First by solving Eq. (45) for ω by replacing the wavenumber in Eq. (45) with the value given by Eq. (52) or (53) and then by applying the result ω and the corresponding wavenumber into Eq. (44), one may obtain the divergence speed which is identical to that (i.e., Eq. (42)) derived by the static eigenvalue problem approach.

Eq. (42) shows that, in theory, the static instability occurs whenever the axial velocity of a beam is equal to the phase speed of the propagating bending wave (i.e., $\omega/\bar{k}_1$) or to the phase speed of the propagating shear wave (i.e., $\omega/\bar{k}_2$). However, in practice, the critical axial velocity of a

Table 1
Comparison of the dimensionless natural frequencies obtained by the present SEM, the FEM, and the exact theory [32]

Dimensionless axial velocity v	Dimensionless axial tension p	Method	$N_E(N_{DOF})$	Dimensionless natural frequency					
				Ω_1	Ω_2	Ω_3	Ω_5	Ω_{10}	Ω_{15}
0	0	Theory 1 [32]	—	1.57	6.28	14.12	39.10	154.45	340.61
		SEM	1 (2)	1.57	6.28	14.12	39.10	154.45	340.61
		FEM	10 (20)	1.57	6.28	14.12	39.28	173.62	433.93
			20 (40)	1.57	6.28	14.12	39.12	155.42	350.20
			50 (100)	1.57	6.28	14.12	39.10	154.53	341.45
			100 (200)	1.57	6.28	14.12	39.10	154.47	340.79
0	4.63×10^{-5}	SEM	1 (2)	1.96	6.71	14.55	39.54	154.90	341.06
		FEM	10 (20)	1.96	6.71	14.56	39.72	174.03	434.31
			20 (40)	1.96	6.71	14.55	39.56	155.86	350.64
			50 (100)	1.96	6.71	14.55	39.54	154.98	341.90
			100 (200)	1.96	6.71	14.55	39.54	154.91	341.24
v_{D1}	4.63×10^{-5}	SEM	1 (2)	0.00	5.67	13.66	38.76	154.14	340.26
		FEM	10 (20)	0.02	5.67	13.68	38.97	173.58	434.44
			20 (40)	0.02	5.67	13.67	38.78	155.17	350.07
			50 (100)	0.02	5.67	13.66	38.76	154.23	341.12
			100(200)	0.02	5.67	13.66	38.76	154.16	340.44

Note: N_E = number of finite elements, $N_{d.o.f}$ = number of d.o.f.

moving beam is usually considered as the lowest divergence speed c_{D1} that is equal to the propagating speed of the first bending wave of the beam.

5. Numerical illustrations and discussions

For numerical illustrations, a uniform beam simply supported at both ends is considered. The geometric and material properties of the beam are the length $L = 1\,\text{m}$, thickness $h = 0.01\,\text{m}$, width $0.03\,\text{m}$, mass per unit length $\rho A = 0.84\,\text{kg/m}$, mass moment of inertia per unit length $\rho I = 7 \times 10^{-6}\,\text{kg m}$, flexural rigidity $EI = 180\,\text{N m}^2$, and the shear rigidity $\kappa GA = 6.75 \times 10^6\,\text{N}$.

Table 1 is prepared to verify the high accuracy of the present spectral element model and also to investigate the effects of dimensionless axial velocity $v = c/\sqrt{E/\rho}$ and dimensionless axial tension $p = P/EA$ on the dimensionless natural frequencies $\Omega_N = \omega_N/(\sqrt{EI/\rho A}/L^2)$. The present spectral element model is evaluated by comparing the natural frequencies obtained by SEM with those obtained by using the exact formula of Blevins [32] and the conventional FEM. The exact formula of Blevins for the natural frequencies of Timoshenko-beam simply supported at both ends is given as follows [32]:

$$\omega_{Np}^2|_{T-beam} = \omega_{Np}^2|_{BE-beam} \frac{L^2 A}{p^2 I}(B - \sqrt{B^2 - D}) \quad (p = 1, 2, 3, \ldots), \tag{54}$$

where p is the mode number and

$$\omega_{Np}|_{BE-beam} = \left(\frac{p\pi}{L}\right)^2 \sqrt{\frac{EI}{\rho A}} \quad \text{(for Bernoulli} - \text{Euler beam)},$$

$$B = \frac{1}{2\pi^2} + \frac{D}{2}\left(\pi^2 + \frac{L^2 A}{p^2 I}\right), \quad D = \frac{\kappa G}{\pi^4 E}. \tag{55}$$

The finite element model used in this study is formulated in the form

$$[\mathbf{M}]\{\ddot{\mathbf{d}}\} + [\mathbf{C}]\{\dot{\mathbf{d}}\} + [\mathbf{K}]\{\mathbf{d}\} = \{\mathbf{f}\}, \tag{56}$$

where $\{\mathbf{d}\}$ is the nodal displacement d.o.f. vector defined by Eq. (20), $\{\mathbf{f}\}$ is the nodal forces vector, $[\mathbf{M}]$ is the mass matrix, $[\mathbf{C}]$ is the skew-symmetric gyroscopic matrix, and $[\mathbf{K}]$ is the stiffness matrix: the finite element matrices are given in Appendix A. To formulate the finite element model given by Eq. (56), the displacement fields within a finite element of length l are assumed in the form [33]

$$w(x,t) = [\mathbf{N}_w(x)]\,\{\mathbf{d}(t)\}, \quad \psi(x,t) = [\mathbf{N}_\psi(x)]\{\mathbf{d(t)}\}, \tag{57}$$

where $[\mathbf{N}_w]$ and $[\mathbf{N}_\psi]$ are the shape function matrices given in Appendix A.

Because the example beam is uniform, only one spectral finite element is used to obtain the SEM results in Table 1, while the total number of convectional finite elements is gradually increased to improve the FEM results. For the case of SEM, the problem size of Eq. (3) is just two by two. In the fourth column of Table 1, the total number of elements and d.o.f.s used for the SEM and FEM results are listed.

Table 1 shows that the SEM results for $v = 0$ and $p = 0$ are identical to the exact analytical results given by Blevins [32], while the FEM results converge to the SEM results (obtained by using one spectral finite element) as the total number of convectional finite elements used in FEM is increased. This implies that, in contrast to the conventional FEM model, the present spectral element model provides highly accurate results by using only a small number of finite elements. This is true especially at high frequency modes. From Table 1, one may observe that, for a fixed axial velocity, the dimensionless natural frequencies are in general increased as the axial tension is increased. On the other hand, for a fixed axial tension, all dimensionless natural frequencies are decreased as the axial velocity of beam is increased. One may also observe from Table 1 that the dimensionless fundamental natural frequency vanishes first when the dimensionless axial velocity v is increased to a certain critical value (i.e., dimensionless divergence speed v_{D1}) at which the static instability (i.e., divergence) occurs.

Table 2 shows the effects of thickness-to-length ratio (h/L) on the dimensionless natural frequencies of the beam. Three beam thicknesses $h = 0.005$, 0.01, and 0.03 m are considered for fixed beam length $L = 1$ m. As the beam thickness is increased, the natural frequencies are found to decrease.

Fig. 2 shows the changes in dimensionless eigenvalues $\Lambda = \lambda/(\sqrt{EI/\rho A}/L^2)$ with varying the dimensionless axial velocity of beam v, for dimensionless axial tension $p = 4.63 \times 10^{-5}$. When the dimensionless axial velocity v is lower than about $v_{D1} = 0.0113$ (the first dimensionless divergence speed), the moving beam is stable because all eigenvalues are pure imaginary. However, if the dimensionless axial velocity is between v_{D1} and $v_s = 0.0194$, there exist pure positive real eigenvalues (i.e., $\mathrm{Re}(\Lambda) > 0$, $\mathrm{Im}(\Lambda) = 0$), which implies the occurrence of the static instability (i.e.,

Table 2
The effects of thickness-to-length ratio (h/L) on the dimensionless natural frequencies of Timoshenko-beam of length $L = 1$ m

Dimensionless axial velocity v	Dimensionless axial tension p	Method	$\frac{h}{L}$	Dimensionless natural frequency					
				Ω_1	Ω_2	Ω_3	Ω_5	Ω_{10}	Ω_{15}
0	0	Theory [32]	0.005	1.57	6.28	14.13	39.23	156.41	350.06
			0.01	1.57	6.28	14.12	39.10	154.45	340.61
			0.03	1.57	6.24	13.94	37.85	137.91	275.51
		SEM	0.005	1.57	6.28	14.13	39.23	156.41	350.06
			0.01	1.57	6.28	14.12	39.10	154.45	340.61
			0.03	1.57	6.24	13.94	37.85	137.91	275.51
0	4.63×10^{-5}	SEM	0.005	3.68	9.16	17.31	42.62	159.91	353.59
			0.01	1.96	6.71	14.55	39.54	154.90	341.06
			0.03	1.58	6.26	13.96	37.86	137.92	275.53
v_{D1}	4.63×10^{-5}	SEM	0.005	0.00	5.74	14.22	39.89	157.42	351.13
			0.01	0.00	5.67	13.66	38.76	154.14	340.26
			0.03	0.00	5.56	13.35	37.27	137.16	274.48

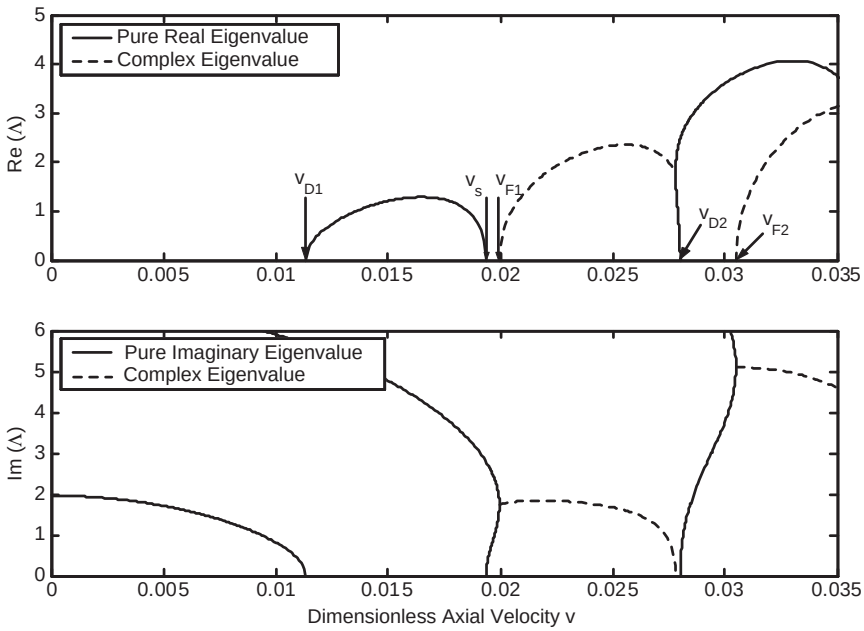

Fig. 2. The dimensionless eigenvalues $\Lambda = \mathrm{Re}(\Lambda) + \mathrm{i}\,\mathrm{Im}(\Lambda)$ vs. the dimensionless axial velocity of beam v, where v_{D1} is the lowest dimensionless divergence speed, v_s is the dimensionless axial velocity at which the second stable region starts, v_{F1} is the lowest dimensionless flutter speed, v_{D2} is the second dimensionless divergence speed, and v_{F2} is the second dimensionless flutter speed.

Table 3
The effects of thickness-to-length ratio (h/L) on the dimensionless critical axial velocities of Timoshenko-beam of length $L = 1\,\mathrm{m}$

$\frac{h}{L}$	Dimensionless critical axial velocity				
	v_{D1}	v_s	v_{F1}	v_{D2}	v_{F2}
0.005	0.011	0.013	0.014	0.017	0.018
0.01	0.011	0.019	0.020	0.028	0.030
0.03	0.027	0.054	0.056	0.081	0.087

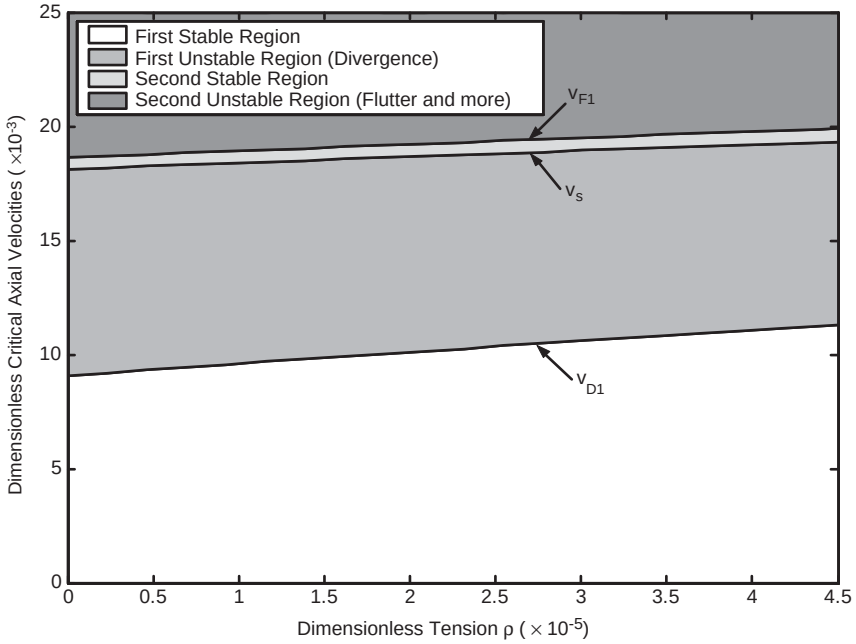

Fig. 3. The critical dimensionless axial velocities vs. the dimensionless axial tension, where v_{D1} is the lowest dimensionless divergence speed, v_s is the dimensionless axial velocity at which the second stable region starts, and v_{F1} is the lowest dimensionless flutter speed.

divergence). Fig. 2 shows that there exist the second stable region between v_s and $v_{F1} = 0.0199$, in which all eigenvalues are pure imaginary. If the dimensionless axial velocity of beam becomes larger than v_{F1}, then there exist dimensionless complex eigenvalues with positive real parts $\mathrm{Re}(\Lambda)$, which implies the occurrence of dynamic instability (i.e., flutter). Thus, v_{F1} is the lowest flutter speed of the example beam. In Fig. 2, $v_{D2} = 0.0280$ is the second dimensionless divergence speed and $v_{F2} = 0.0305$ is the second dimensionless flutter speed. Table 3 shows the effects of the thickness-to-length ratio (h/L) on the dimensionless critical axial velocities indicated in Fig. 2. As the thickness-to-length ratio is increased, it is found that the critical axial velocities tend to increase.

Fig. 3 shows the changes in three critical dimensionless axial velocities of beam, v_{D1} (the lowest dimensionless divergence speed), v_s, and v_{F1} (the lowest dimensionless flutter speed) with varying

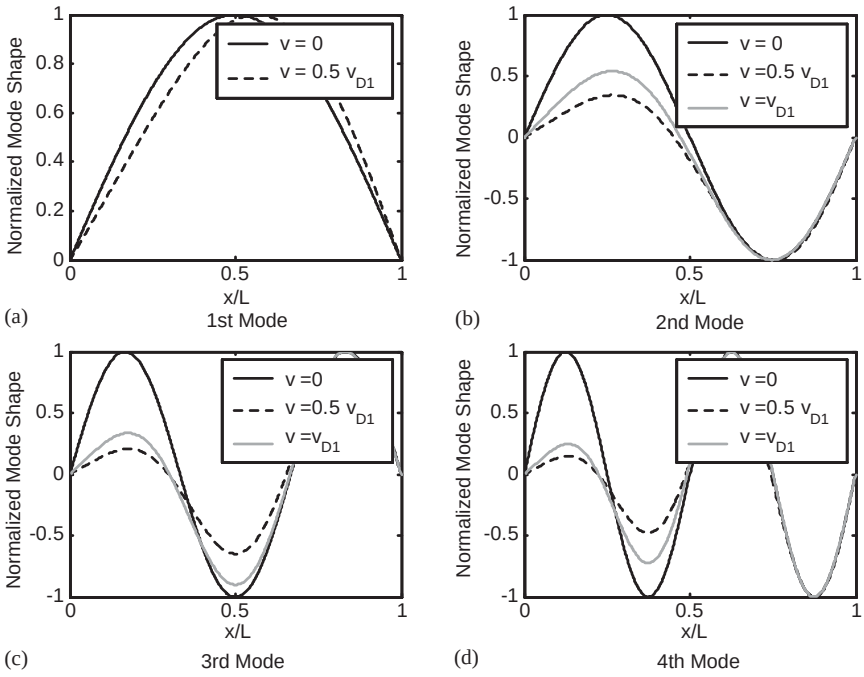

Fig. 4. Dimensionless axial velocity dependence of the natural modes of a moving Timoshenko-beam under the dimensionless axial tension $p = 4.63 \times 10^{-5}$.

the dimensionless axial tension p. The region below the curve v_{D1} and the narrow region between two curves v_s and v_{F1} are the first stable region and the second stable region, respectively. The region between two curves v_{D1} and v_s indicates the first divergence instability region, while the region just above the curve v_{F1} indicates the flutter instability region. It is apparent from Fig. 3 that the three critical dimensionless axial velocities are monotonically increased as the dimensionless axial tension is increased.

The moving Thimoshenko beam may have complex natural modes. Fig. 4 compares the real parts of the natural modes for various dimensionless axial velocities. It shows that the symmetric or antisymmetric natural modes of the stationary beam are all distorted due to the effects of axial velocity and thus their original symmetry or antisymmetry cannot be reserved for the case of moving beam. In Table 1, it is shown that the fundamental dimensionless natural frequency of bending mode vanishes when the dimensionless axial velocity of beam reaches at the dimensionless divergence speed v_{D1}. Accordingly, one may observe from Fig. 4(a) that the first bending mode indeed disappears when the beam is axially traveling at the dimensionless axial velocity of v_{D1}.

Fig. 5 shows the dispersion curves for the stationary Timoshenko beam. There exist the propagating bending wave (k_1) and evanescent wave (k_2) below the cut-off frequency $\Omega_c = 10677$, while there exists only the propagating shear wave (k_2) above the cut-off frequency Ω_c.

Fig. 6 shows the changes in the dispersion curves of the moving Timoshenko beam with varying its dimensionless axial velocity. The lowest two dimensionless natural frequencies are indicated in

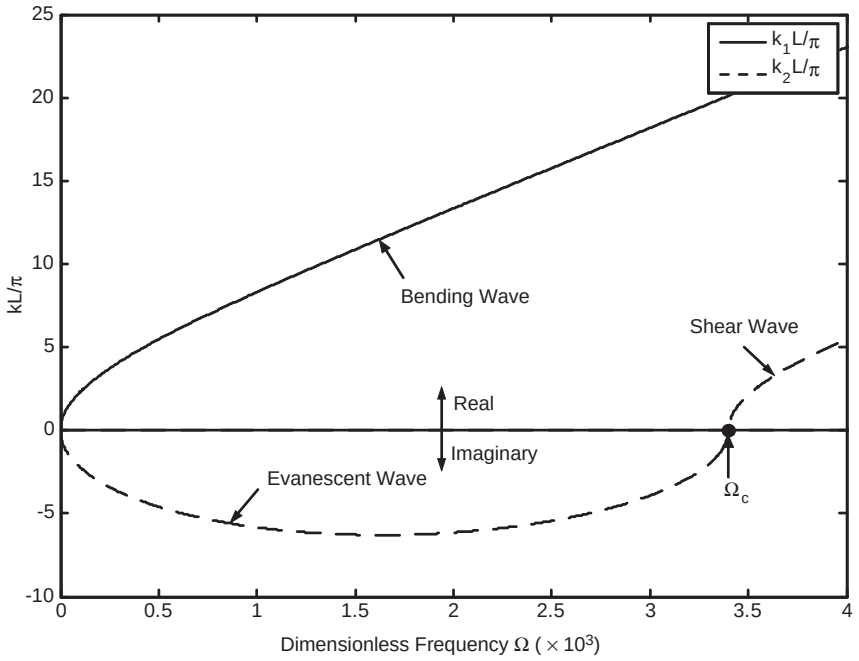

Fig. 5. Dispersion relation for the stationary Timoshenko-beam (i.e., $v = 0$) under the dimensionless axial tension $p = 4.63 \times 10^{-5}$, where Ω_c is the dimensionless cut-off frequency.

Fig. 6 by the circle (○) and the triangle (Δ), in order to show they all move to leftward as the dimensionless axial velocity of beam is increased. As shown in Fig. 6(e), the fundamental dimensionless natural frequency Ω_1 vanishes first when the dimensionless axial velocity reaches at $v_{D1} = 0.0113$ and then it disappears forever as the dimensionless axial velocity is increased over v_{D1}. When the beam is in the stationary state (i.e., $v = 0$), the wavenumber k_2 is pure imaginary and there exists evanescent wave within the beam as shown in Fig. 6(a). However, when the beam is moving, wavenumber k_2 becomes complex as shown in Fig. 6(b). As the dimensionless axial velocity of beam is increased up to $v_{LC} = 0.0068$, all wavenumers at zero frequency merge to zeros (see Fig. 6c). If the dimensionless axial velocity of beam is kept increasing over v_{LC}, the wavenumber k_2 becomes pure real at $0 \leqslant \Omega \leqslant \Omega_{LC}$, while it is complex at $\Omega \geqslant \Omega_{LC}$. This implies that, when the dimensionless axial velocity is lager than v_{LC}, there exits traveling shear wave within a narrow low-frequency band given by $0 \leqslant \Omega \leqslant \Omega_{LC}$. Thus, the dimensionless frequency Ω_{LC} is the dimensionless lower cut-off frequency which is far below the dimensionless cut-off frequency Ω_C shown in Fig. 5. The dimensionless lower cut-off frequency Ω_{LC} and the critical dimensionless axial velocity v_{LC} above that the dimensionless lower cut-off frequency may exist can be derived from Eq. (14) as

$$\Omega_{LC} = \frac{1}{2\pi}\sqrt{\frac{-f_2 - \sqrt{f_2^2 - 4f_1f_3}}{2f_1}}\Big/\frac{1}{L^2}\sqrt{\frac{EI}{\rho A}}, \quad v_{LC} = \sqrt{\frac{P}{EA}}, \tag{58}$$

where f_1, f_2, and f_3 are given in Appendix B.

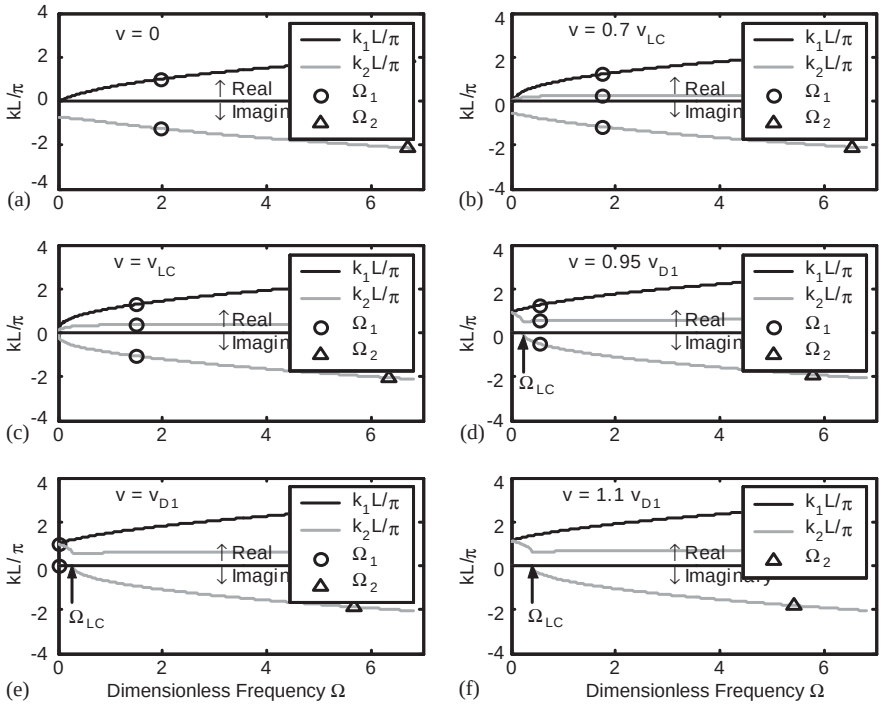

Fig. 6. Dimensionless axial velocity dependence of the dispersion relation of a moving Timoshenko-beam under the dimensionless axial tension $p = 4.63 \times 10^{-5}$, where $\bigcirc$ and Δ indicate the 1st and 2nd dimensionless natural frequencies, respectively, and Ω_{LC} is the lower dimensionless cut-off frequency which appears when $v \geqslant v_{LC}$.

6. Conclusions

In the present paper, the dynamic equations of motion for the moving Timoshenko beam under a uniform axial tension are derived and then the spectral element model is formulated by using the exact dynamic shape functions. The high accuracy of the present spectral element is then verified by comparing its solutions with the exact analytical solutions and the conventional FEM solutions. The critical axial velocity at which the divergence instability occurs is analytically derived in a closed form. Through some numerical studies are conducted to investigate the followings:

The axial tension tends to decrease the natural frequencies while the axial velocity increases them. When the moving speed equals to the lowest divergence speed given by Eq. (42), the fundamental natural frequency vanishes to make the first bending mode disappear with inducing the static instability.

There may exist a very narrow stable region between the first static instability (divergence) region and the first dynamic instability (flutter) region. The divergence and flutter speeds tend to increase as the axial tension is increased.

When the axial velocity is larger than the value of $\sqrt{P/\rho A}$, there exist a lower cut-off frequency below that the propagating shear wave appears.

Appendix A

The shape function matrices used in Eq. (57) are defined by [33]

$$\begin{aligned}[\mathbf{N}_w(x)] &= [(1-\xi)(2-\xi-\xi^2+6r)R/4, l(1-\xi^2)(1-\xi+3r)R/8,\\ &\quad (1+\xi)(2+\xi-\xi^2+6r)R/4, l(1-\xi^2)(1+\xi+3r)R/8],\\ [\mathbf{N}_\psi(x)] &= [-3(1-\xi^2)R/(2l), -(1-\xi)(1+3\xi-6r)R/4,\\ &\quad 3(1-\xi^2)R/(2l), -(1+\xi)(1-3\xi-6r)R/4],\end{aligned} \tag{A.1}$$

where

$$\xi = 2\left(\frac{x}{l}\right) - 1 \quad (0 \leqslant x \leqslant l), \quad r = \frac{4EI}{\kappa GAl^2}, \quad R = \frac{1}{1+3r}. \tag{A.2}$$

The finite element matrices in Eq. (56) are derived in the form

$$[\mathbf{M}] = [m_{ij}] = [m_{ij}]^{\mathrm{T}}, \quad [\mathbf{C}] = [c_{ij}] = -[c_{ij}]^{\mathrm{T}}, \quad [\mathbf{K}] = [k_{ij}] = [k_{ij}]^{\mathrm{T}} \quad (i,j = 1,2,3,4) \tag{A.3}$$

with the components given by

$$\begin{aligned}
m_{11} &= m_{33} = 12m_T(26+147r+210r^2) + 36m_R,\\
m_{12} &= -m_{34} = m_T l(44+231r+315r^2) + 3m_R l(1-15r),\\
m_{13} &= 36m_T(3+21r+35r^2) - 36m_R,\\
m_{14} &= -m_{23} = -m_T l(26+189r+315r^2) + 3m_R l(1-15r),\\
m_{22} &= m_{44} = m_T l^2(8+42r+63r^2) + m_R l^2(4+15+90r^2),\\
m_{24} &= -3m_T l^2(2+14r+21r^2) - m_R l^2(1+15r-45r^2),\\
m_T &= \rho AlR^2/840, \quad m_R = \rho IR^2/(30l),
\end{aligned}$$

$$\begin{aligned}
c_{11} &= c_{22} = c_{33} = c_{44} = 0,\\
c_{12} &= c_{23} = c_{34} = -c_{14} = 3c_T l(2+5r) + 2c_R,\\
c_{24} &= -c_T l^2 - c_R l(1-3r),\\
c_T &= c\rho AlR/30, \quad c_R = c\rho IR/l,
\end{aligned} \tag{A.4}$$

$$\begin{aligned}
k_{11} &= -k_{13} = k_{33} = 4R^2[k_O + 3k_R + 9k_T(2+10r+15r^2)],\\
k_{12} &= k_{14} = -k_{23} = -k_{34} = 2lR^2(k_O + 3k_R + 3k_T),\\
k_{22} &= k_{44} = l^2R^2[k_O + k_R(4+6r+9r) + k_T(8+30r+45r^2)],\\
k_{24} &= l^2R^2[k_O + k_R(2-6r-9r^2) + k_T(2+30r+45r^2)],\\
k_O &= 9rEI/l^3, \quad k_R = (EI - c^2\rho I)/l^3, \quad k_T = (P - c^2\rho A)/(60l).
\end{aligned}$$

Appendix B

In Eq. (58), f_i $(i = 1, 2, 3)$ are defined by

$$\begin{aligned}
f_1 = & -8a_1^2c^6[a_5^2a_2^3(a_5+1)+a_1a_2^2a_5a_6(a_5-4)+a_2(a_1a_6)^2(1-4a_5)+2(a_1a_6)^3] \\
& -4a_1c^4[a_2^3a_5^2(a_5-1)(3a_5+2)+a_1a_2^2a_5a_6(7a_5^2-12a_5+8) \\
& -2a_2(a_1a_6)^2(9a_5^2-4a_5+1)(a_1a_6)^3(8a_5-5)] \\
& +c^2[-a_2^3a_5^2(a_5-1)^2(4a_5-1) \\
& -a_1a_2^2a_5a_6(a_5-1)(5a_5+2)(6a_5-5) \\
& +a_2(a_1a_6)^2(5a_5^3-33a_5^2-36a_5+1)+(a_1a_6)^3(13a_5-22a_5^2-3)] \\
& -2a_5a_6[a_2^2a_5(5a_5-2)(a_5-1)^2-2a_1a_2a_6(4a_5^2 \\
& +a_5-1)(a_5-1)+(a_1a_6)^2(3a_5^2+2a_5+3)], \\
f_2 = & \, a_1a_3c^4[(a_2a_5)^2(a_5-1)^2+2a_1a_2a_5a_6(4a_5^2+a_5-5) \\
& +(a_1a_6)^2(1-20a_5-8a_5^2)]+a_3(a_5-1)c^2[(a_2a_5)^2(a_5-1)^2 \\
& +a_1a_2a_5a_6(a_5-1)(13a_5+10)+(a_1a_6)^2(1-25a_5-12a_5^2)] \\
& +a_3a_5a_6(a_5-1)^2[a_2(a_5-1)(5a_5-1)-4a_1a_6(a_5+1)], \\
f_3 = & \, a_3^2a_5a_6(a_5+1)^3(a_1c^2-a_5-1),
\end{aligned} \tag{B.1}$$

where

$$a_5 = 1 + a_4 - a_1c^2, \quad a_6 = 1 - a_2c^2. \tag{B.2}$$

References

[1] J.A. Wickert, C.D. Mote Jr., Current research on the vibration and stability of axially moving materials, Shock and Vibration Digest 20 (1988) 3–13.

[2] F. Pellicano, F. Vestroni, Non-linear dynamics and bifurcations of an axially moving beam, Journal of Vibration and Acoustics 122 (2001) 21–30.

[3] C.D. Mote Jr., A study of band saw vibrations, Journal of the Franklin Institute 279 (4) (1965) 430–444.

[4] C.D. Mote Jr., S. Naguleswaran, Theoretical and experimental band saw vibrations, Journal of Engineering for Industry 88 (1966) 151–156.

[5] K.W. Wang, C.D. Mote, Vibration coupling analysis of band/wheel mechanical systems, Journal of Sound and Vibration 102 (1) (1986) 1–9.

[6] S.J. Hwang, N.C. Perkins, Supercritical stability of an axially moving beam, Parts I and II, Journal of Sound and Vibration 154 (3) (1992) 381–409.

[7] A.A.N. Al-Jawi, C. Pierre, A.G. Ulsoy, Vibration localization in dual-span axially moving beams, Part I: formulation and results, Journal of Sound and Vibration 179 (2) (1995) 243–266.

[8] K.D. Murphy, Y. Zhang, Vibration and stability of a cracked translating beam, Journal of Sound and Vibration 237 (2) (2000) 319–335.

[9] F. Pellicano, A. Fregolent, A. Bertuzzi, F. Vestroni, Primary and parametric non-linear resonance of a power transmission belt: experimental and theoretical analysis, Journal of Sound and Vibration 244 (4) (2001) 669–684.

[10] H.P. Lee, Dynamics of a beam moving over multiple supports, International Journal of Solids and Structures 30 (2) (1993) 199–209.
[11] M. Stylianou, B. Tabarrok, Finite element analysis of an axially moving beam, Part I: time integration, Journal of Sound and Vibration 178 (4) (1994) 433–453.
[12] T.R. Sreeram, N.T. Sivaneri, FE-analysis of a moving beam using Lagrangian multiplier method, International Journal of Solids and Structures 35 (28–29) (1998) 3675–3694.
[13] J.A. Wickert, C.D. Mote Jr., Classical vibration analysis of axially moving continua, Journal of Applied Mechanics 57 (1990) 738–744.
[14] C.H. Riedel, C.A. Tan, Dynamic characteristics and mode localization of elastically constrained axially moving strings and beams, Journal of Sound and Vibration 215 (3) (1998) 455–473.
[15] A.L. Thurman, C.D. Mote Jr., Free, periodic, nonlinear oscillation of an axially moving strip, Journal of Applied Mechanics 36 (1969) 83–91.
[16] H.R. Öz, M. Pakdemirli, Vibrations of an axially moving beam with time-dependent velocity, Journal of Sound and Vibration 227 (2) (1999) 239–257.
[17] H.R. Öz, On the vibrations of an axially traveling beam on fixed supports with variable velocity, Journal of Sound and Vibration 239 (3) (2001) 556–564.
[18] J.A. Wickert, Non-linear vibration of a traveling tensioned beam, International Journal of Non-Linear Mechanics 27 (3) (1992) 503–517.
[19] E. Özkaya, M. Pakdemirli, Vibrations of an axially accelerating beam with small flexural stiffness, Journal of Sound and Vibration 234 (3) (2000) 521–535.
[20] B. Tabarrok, C.M. Leech, Y.I. Kim, On the dynamics of an axially moving beam, Journal of the Franklin Institute 297 (8) (1974) 201–220.
[21] Y.K. Wang, C.D. Mote Jr., Active and passive vibration control of an axially moving beam by smart hybrid bearings, Journal of Sound and Vibration 195 (4) (1996) 575–584.
[22] S.Y. Lee, C.D. Mote Jr., A generalized treatment of the energetics of translating continua, Part II: beams and fluid conveying pipes, Journal of Sound and Vibration 204 (5) (1997) 735–753.
[23] S.Y. Lee, C.D. Mote Jr., Wave characteristics and vibration control of translating beams by optimal boundary damping, Journal of Vibration and Acoustics 121 (1999) 18–25.
[24] G. Chakraborty, A.K. Mallik, Wave propagation in and vibration of a traveling beam with and without non-linear effects, Part I: free vibration, Part II: forced vibration, Journal of Sound and Vibration 236 (2) (2000) 277–305.
[25] Y. Li, C.D. Rahn, Adaptive vibration isolation for axially moving beams, IEEE/American Society of Mechanical Engineers Transactions on Mechatronics 5 (4) (2000) 419–428.
[26] Y.I. Kwon, J.G. Ih, Vibration power flow in the moving belt passing through a tensioner, Journal of Sound and Vibration 229 (2) (2000) 329–353.
[27] A. Simpson, Transverse modes and frequencies of beams translating between fixed end supports, Journal of Mechanical Engineering Science 15 (1973) 159–164.
[28] S. Chonan, Steady state response of an axially moving strip subjected to a stationary lateral load, Journal of Sound and Vibration 107 (1) (1986) 155–165.
[29] J.F. Doyle, Wave Propagation in Structures: Spectral Analysis Using Fast Discrete Fourier Transforms, Springer, New York, 1997.
[30] U. Lee, J. Kim, A.Y.T. Leung, The spectral element method in structural dynamics, The Shock and Vibration Digest 32 (6) (2000) 451–465.
[31] L. Le-Ngoc, H. McCallion, Dynamic stiffness of an axially moving string, Journal of Sound and Vibration 220 (4) (1999) 749–756.
[32] R.D. Blevins, Formulas for Natural Frequency and Mode, Van Nostrand Reinhold Company, New York, 1979.
[33] M. Petyt, Introduction to Finite Element Vibration Analysis, Cambridge University Press, New York, 1990.
[34] R.L. Bisplinghoff, H. Ashley, Principles of Aeroelasticity, Dover Publications, New York, 1962.
[35] C.C. Lin, Stability and vibration characteristics of axially moving plates, International Journal of Solids and Structures 34 (24) (1997) 3179–3190.